Reactivity of ZnO Surfaces toward Maleic Anhydride

Stefanie Gil Girol,† Thomas Strunskus,† Martin Muhler,‡ and Christof Wöll*,†

Lehrstuhl für Physikalische Chemie I and Lehrstuhl für Technische Chemie, Ruhr-Universität Bochum, 44780 Bochum, Germany

Received: April 13, 2004; In Final Form: June 18, 2004

In this work, the adsorption and temperature induced-decomposition of maleic anhydride (MA, $C_4H_2O_3$) on the polar Zn−ZnO(0001) and O−ZnO(000$\bar{1}$) surfaces and on the nonpolar ZnO(10$\bar{1}$0) surface of zinc oxide were investigated using X-ray photoelectron spectroscopy (XPS) and near-edge X-ray absorption fine structure (NEXAFS). Despite the fact that molecules such as small hydrocarbons, alcohols, aldehydes, and carboxylic acids are generally reported to show higher reactivities on the Zn-terminated polar surface than on the O-terminated polar surface, we find that the temperature-induced decomposition of MA is essentially the same on both polar surfaces as well as on the mixed-terminated surface. In the case of the O-terminated surface, it was possible to correlate the defect density with the observed reactivity. Hence, regarding MA decomposition, the defect density seems to play a major role for the catalytic activity.

Introduction

Maleic anhydride ($C_4H_2O_3$, MA) is a versatile raw material that is used for the production of polymers, agricultural chemicals, pharmaceutical products, lubricant additives, surfactants, and plasticizers.[1]

One of the most important products made from MA is 1,4-butanediol (BDL), which is produced by hydrogenation of MA over Cu/ZnO catalysts. BDL plays a major role for the fabrication of technologically important polymers such as polyurethanes and polybutylene terephthalate used in engineering plastics, films, fibers and adhesives, as well as for the production of the solvents γ-butyrolactone and tetrahydrofurane.[1] Only five years ago, the majority of BDL was still produced by the Reppe process[2,3] which is based on the reaction of acetylene with formaldehyde, although several disadvantages, such as hazardous starting materials, severe reaction conditions, and a multistep reaction pathway, render this synthesis route unfavorable.

The commercial hydrogenation of MA and related dialkyl maleates over Cu/ZnO catalysts was established in the 90s, and a large number of investigations dealing with the catalyst composition and the reaction conditions have been published so far.[4−11] Still, there is a lack of surface-analytical studies of the MA/Cu/ZnO system providing an understanding of the catalytic processes on a microscopic scale.

The hydrogenation of MA over Cu/ZnO catalysts, which is industrially performed either in the liquid phase or in the vapor phase, follows the reaction scheme shown in Figure 1. The conversion of MA proceeds via succinic anhydride which is then hydrogenated to γ-butyrolactone (GBL) and further to BDL. Tetrahydrofurane (THF) can be produced by dehydration of BDL[4,7,8,12] or directly from GBL.[6] The yield of this hydrogenation process is a mixture of the high value products GBL, THF, and BDL. Typically, methanol, ethanol, propanol, butanol, propionic and butyric acid, as well as methane and

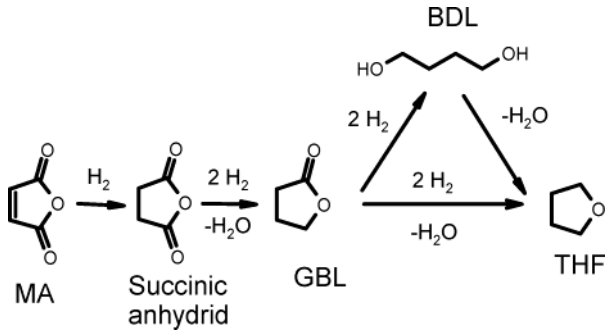

Figure 1. Reaction pathway for the liquid phase and vapor phase hydrogenation of maleic anhydride (MA).[4−8,12]

acetylene[6,9,10] are found as byproducts in the hydrogenation process. The catalysts used in the cited publications are commercially available Cu/ZnO/Al_2O_3 catalysts[4,7,8] as well as catalysts prepared by coprecipitation of Cu and Zn carbonates yielding spinel-type compounds.[5,6]

According to the literature,[6,7,9] the catalytic activity of the Cu/ZnO catalyst for each hydrogenation step can be attributed exclusively to copper. However, ZnO-free copper catalysts do not yield the desired BDL; that is, after formation of GBL, further hydrogenation of GBL is not observed. This finding is explained by a competitive adsorption of succinic anhydride and GBL on the active copper surface, which forces GBL to desorb from the surface and inhibits its readsorption. When ZnO is added to the catalyst mixture, the hydrogenation of GBL is assumed to continue following the reaction scheme in Figure 1. This behavior is attributed to the idea that ZnO provides additional sorption sites for succinic anhydride, so that its coverage on the active copper surface is reduced. This enables readsorption and reaction of GBL at the active Cu sites so that the hydrogenation to BDL is completed.

In this study, we have investigated the adsorption behavior of maleic anhydride (MA) on the polar (0001) and (000$\bar{1}$) surfaces as well as on the nonpolar (10$\bar{1}$0) surface of ZnO using XPS (X-ray photoelectron spectroscopy) and NEXAFS (near-edge X-ray absorption fine structure) spectroscopy. No

* To whom correspondence should be addressed. E-mail: woell@pc.rub.de.
† Lehrstuhl für Physikalische Chemie I.
‡ Lehrstuhl für Technische Chemie.

10.1021/jp048386d CCC: $27.50
Published on Web 08/12/2004

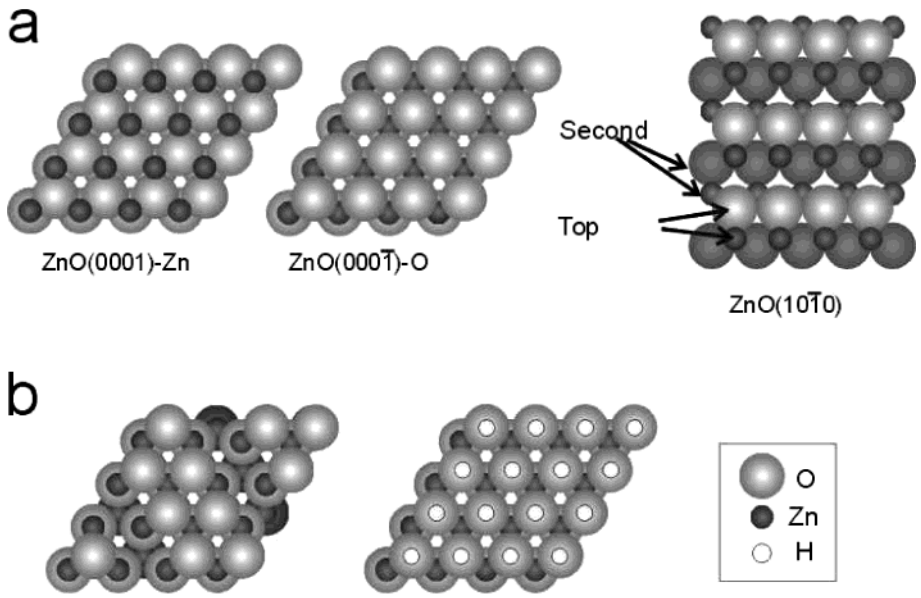

Figure 2. Models showing the ideal polar surfaces and the ideal (10$\bar{1}$0)-surface of ZnO (a) as well as the surface structures of the O-terminated surface as derived from experimental data[26−28] (b). The (3×1) missing row structure which is found at higher temperatures transforms into the H(1 × 1) phase at lower temperatures due to water (or hydrogen) uptake.

previous studies of MA on ZnO single crystals have been published to the best of our knowledge. However, investigations of MA on a metal oxide, TiO_2(001), and on metal surfaces such as Mo(110) and Pd(111) have been reported in the literature.

Idriss et al.[13] have investigated the decomposition of MA on TiO_2(001) surfaces. Their TDS results indicate two different reaction pathways both following adsorption under formation of a seven-membered ring by insertion of a substrate TiO-pair into the anhydride group. The formation of this species was also supported by PM3 semiempirical cluster calculations. Decomposition was found to occur upon heating, yielding considerable amounts of ketene, CO, CO_2, and acetylene. On Ar^+-sputtered surfaces the fraction of C4 and C6-products was found to increase, suggesting that the chemistry becomes less selective with increasing defect density.

On Mo(110), irreversible adsorption of MA was found by Xu and Goodman.[14] This was concluded from TDS experiments where fragmentation into CO, CO_2, H_2, and adsorbed carbon was observed. HREELS results suggest adsorption through the ring oxygen atom involving a weakening or scission of one adjacent bond with the molecular plane being essentially normal to the surface. A different adsorption geometry was found on bimetallic Pd/Mo(110) surfaces. For a Pd monolayer on Mo-(110) and for an epitaxially grown Pd (111) multilayer on Mo, the authors report adsorption through the olefin bond in a π bound and a di-σ bound configuration, respectively. On these surfaces, the fraction of decomposed MA amounts to only 15−20%. The lower decomposition degree on the Pd surfaces is attributed to the fact that the affinity of Pd toward oxygen is lower than that of Mo.

In agreement with the previous findings, DFT calculations for MA on a Pd(111) cluster performed by Pallassana et al.[15] indicate that at low coverages the most favorable chemisorption mode is the di-σ bound configuration. The theoretical binding energy shows good agreement with the experimental value found by Xu and Goodman.[14]

The adsorption behavior of MA on Si(100)-2×1 was investigated by Richardson et al.[16,17] using NEXAFS, HREELS, LEED, and STM. At low coverages, adsorption in a di-σ configuration was found resulting in a bidentate species with a rehybridized sp^3 olefin bond, whereas at high coverages a monodentate species was proposed, which is bound to the surface through a Si−C bond following C−H bond cleavage. Fragmentation of MA was not observed on the Si(100)-2×1 surface.

Although no comparable studies have been performed for MA adsorbed on ZnO surfaces, the interaction of a variety of other molecules with this material has been investigated.[12,18−25] The surface chemistry observed strongly depends on the structural and electronic properties of the particular ZnO single-crystal surfaces. Figure 2a shows the surface structures of the ideal, polar O-terminated (000$\bar{1}$), and Zn-terminated (0001) surfaces and the mixed-terminated (10$\bar{1}$0) surface. As can be expected, especially the O- and Zn-terminated faces exhibit a clearly distinct behavior. Oxygen-containing molecules that possess strong dipole moments are reported to interact most strongly with the Zn-terminated surface, less with the nonpolar and least strongly with the O-terminated surface.[18] The dehydrogenation of alkynes was also found to depend on the surface termination since on the Zn-face proton abstraction occurred whereas on the O-face only molecular adsorption was observed.[23] The decomposition behavior of acetic and propionic acid was reported to follow the same trend. Molecular adsorption on the O-face contrasts formation of a carboxylate species on the Zn-face which at higher temperatures is decomposed via dehydrogenation (resulting in ketene and acrolein, respectively) or via formation of CO_2 and adsorbed alkyl species. In a final step, the latter are dehydrogenated to leave atomic carbon on the surface.[24]

In addition to the differing electronic properties of the polar surfaces that affect the interaction with particular adsorbates, the structural properties play a major role. Since the decomposition reactions are thought to proceed via acid−base pathways, the accessibility of zinc−oxygen pairs should be a determining factor for the catalytic activity of the related surface. The lack of reactivity of the O-face can be attributed to the fact that zinc ions in the second layer are more effectively shielded by the larger O-atoms in the top layer, than vice versa on the Zn-terminated polar (0001) surface. In correlation with this, also

imperfections such as oxygen vacancies and steps have to be considered to be a determining factor for the reactivities of the surfaces.

Regarding the O-terminated surface, recent studies have revealed the presence of a hydroxyl-terminated H(1×1)O−ZnO surface under UHV conditions at room temperature.[26,27] There was no evidence for a clean (1×1)-ordered O-terminated surface. Instead, at high temperatures, a (1×3)-reconstruction was observed which is attributed to a missing row structure caused by oxygen vacancies, see Figure 2b. Under the conditions of the present study the O-terminated surface was always fully hydroxylated.

Experimental Section

The experiments were performed in two different UHV systems. The apparatus used for the XPS experiments was equipped with a modified Leybold XPS system, an EA11 hemispherical energy analyzer, and an Omicron LEED system. The base pressure of the apparatus was below 1×10^{-10} mbar. NEXAFS experiments were carried out in a different apparatus, containing a VG XPS system, a VG LEED system, and a Leybold sputtergun. NEXAFS spectra were recorded in the partial electron yield mode using a channel plate detector. The base pressure of this system was below 5×10^{-10} mbar. One of the crystals under investigation, the O-terminated crystal later referred to as "defect rich", was investigated at BESSY I at the beamline HE-TGM2, whereas the second O-terminated crystal, referred to as "near stoichiomeric", was examined at the beamline HE-SGM at BESSY II. The degree of polarization of the synchrotron radiation amounts to 80%.

All ZnO samples used in this study were cut with an accuracy of ±0.2° and polished mechanically. After introduction into the UHV system a standard preparation procedure was applied to clean the samples. Repeated cycles of Ar^+ ion bombardment (1×10^{-4} mbar Ar, 750 V, 1.5 μA, 4h) at 650 K were followed by annealing at 850 K in an O_2 ambient (1×10^{-6} mbar, 15 min). The cleanliness of the samples was monitored by XPS. Typically after 15 preparation cycles impurities could not be detected anymore (XPS detection limit for carbon ~1 at. %[29]). The quality of the surfaces was controlled by LEED.

Atomic hydrogen was produced by backfilling the preparation chamber with molecular hydrogen (1×10^{-6} mbar) and operating a hot tungsten filament in direct line of sight with the crystal surface at a distance of approximately 5 cm.

The sample temperature was measured by a Ni/NiCr-thermocouple tightly clamped to the edge of the crystals and controlled by a PID circuit. Cooling with liquid nitrogen allowed crystal temperatures below 150 K.

Prior to the adsorption experiments maleic anhydride (supplied by Aldrich) was purified by sublimation. Due to its high vapor pressure, dosage was carried out by backfilling the chamber through a leak valve. The dosage is given in Langmuir ($1L = 1 \times 10^{-6}$ Torr × 1 s).

The XP spectra were fitted using Gaussian peaks after subtraction of a linear background. The line widths amounted to 1.45, 1.6, and 2.0 eV for the C1s, O1s, and Zn2p lines, respectively. The thickness d of the deposited MA layers was estimated from the attenuation of the substrate $Zn2p_{3/2}$ XPS line using the equation $d = \lambda_{Zn} \cdot \ln[I_{Zn,clean}/I_{Zn,ads}] \cdot I_{Zn,clean}$ and $I_{Zn,ads}$ are the intensities of of the $Zn2p_{3/2}$ line of the clean substrate and the substrate with adsorbate, respectively. λZ_n is the inelastic mean free path of the $Zn2p_{3/2}$ photoelectrons in MA, which amounts to 16 ± 2 Å as estimated from the predictive formula of Tanuma et al.[30] The number of adsorbed layers was calculated by assuming that the coverage on the ZnO($10\bar{1}0$) surface at 160 K corresponds to approximately 1 monolayer.

TABLE 1: NEXAFS Resonances Observed for MA Multilayers on O−ZnO[a]

	resonance	transition	observed photon energy [eV]
carbon edge	1	π_1^*(C=C)	284.0
	2	π_1^*(C=O)	287.9
		π_2^*(C=C)	
	3	π_3^*(C=C)	288.6
	4	π_2^*(C=O)	290.2
	5	π_3^*(C=O)	291.8
oxygen edge	6	π_1^*(C=O)	531.0
	7	π_2^*(C=O)	534.0
	8	π_3^*(C=O)	535.8

[a] The assignments are taken from the work of Lopez et al.[16]

The evaluation of the adsorbate NEXAFS spectra included correction of both the sample spectrum and the clean substrate spectrum for the transmission function by division through the NEXAFS spectrum of a clean gold substrate prior to normalization of both spectra in the low energy regime. In the following, the clean substrate spectrum is subtracted from the sample spectrum. The resulting adsorbate spectrum is then normalized to the edge jump.

The energy positions and the assignment of the π^* NEXAFS resonances are shown in Table 1. The labeling of the resonances, π_n^*, follows that used in previous work.[16]

Results

XPS. In a first set of experiments the thermal stability of MA on the different ZnO surfaces was monitored using XPS. After deposition of the adsorbate at crystal temperatures below 170 K the temperature was raised stepwise to at least 600 K. XP spectra of the O1s, C1s and Zn2p regions were recorded at each temperature step.

XPS allows a straightforward distinction of the different C and O species present in the MA molecule (see Figure 1) due to their significantly different chemical shifts (see, e.g., Figure 3). In the C1s region, the olefinic (286.3 eV) and carbonyl carbon signals (290.0 eV) are separated by 3.7 eV. In the O1s regime, the line related to carbonyl oxygen (533.2 eV) is found to be about 1.4 eV lower than that corresponding to anhydride oxygen (534.6 eV). The O1s peak of the ZnO substrate (530.7 eV) appears 2.5 eV below the carbonyl line. In all subsequent spectra, this substrate peak was subtracted. In some cases, this procedure leads to the appearance of artifacts in the O1s difference spectra located at 530 eV. The subtraction procedure is demonstrated in Figure 3 where the original spectrum as well as the same spectrum after subtraction of the fitted O1s substrate line are displayed.

XPS of MA Deposited on Zn−ZnO. Figure 3 shows a series of C1s and O1s spectra recorded for MA deposited on the Zn−ZnO surface. At 165 K, the crystal was exposed to 95 L MA, resulting in a coverage of approximately 2 layers.

The XP spectra recorded at 165 and 180 K reflect the stoichiometry of intact MA. Regarding the C1s region, the multilayer spectra can be fitted using two lines of equal intensity at 286.3 and 290.0 eV. The two additional lines of smaller intensity at 288.5 and 285.1 eV are attributed to parts of the monolayer as explained below (compare, e.g., with the results obtained on the ($10\bar{1}0$)-terminated ZnO surface where the initial coverage was in the monolayer range). In the O1s regime, the fit with two Gaussian peaks at 533.2 and 534.6 eV yields

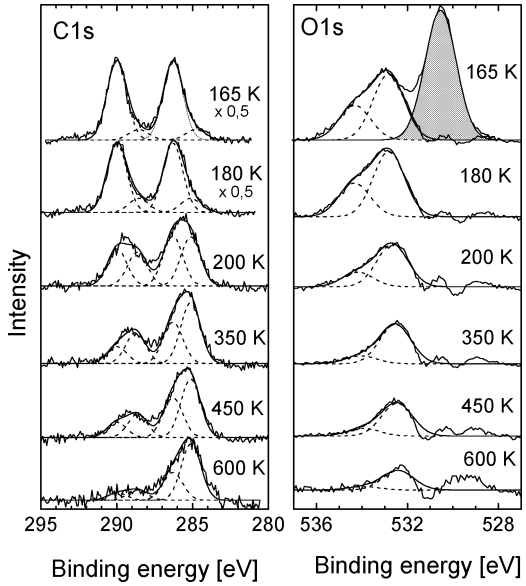

Figure 3. XPS series of MA on Zn−ZnO(0001). In the O1s spectrum at the top, the subtraction of the O1s substrate line is demonstrated. The fitted O1s substrate signal (grey area) is subtracted from the original data.

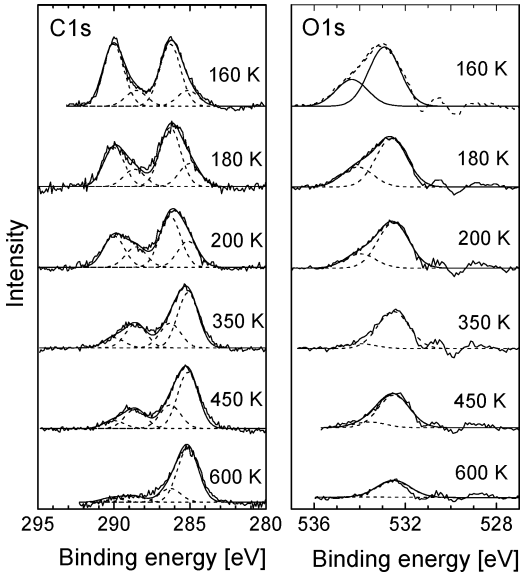

Figure 4. XPS series of MA on ZnO(10$\bar{1}$0).

good agreement with the experimental data. As expected for intact molecules, the carbonyl to anhydride oxygen ratio amounts to 2:1.

The temperature increase to 200 K leads to multilayer desorption, resulting in a general intensity decrease of the adsorbate lines. In this monolayer regime, the intensity of the C1s lines at 290.0 and 286.3 eV decreases while the lines at 288.5 and 285.1 eV become more pronounced. The intensity ratio of carbonyl carbon (with lines at 290.0 and 288.5 eV) and olefinic carbon (with lines at 286.3 and 285.1 eV) drops from 1:1 to about 0.6:1, and the intensities of the carbonyl and anhydride oxygen lines both decrease with respect to the intensities observed at 180 K. This behavior clearly indicates a fragmentation of the adsorbed monolayer, accompanied by a loss of carbonyl or carboxyl groups. Since at 200 K there is still a contribution of the XPS lines characteristic for the intact molecule, it can be assumed that intact molecules as well as decomposition products coexist at this temperature.

In the temperature regime between 200 and 600 K, the decomposition of the monolayer proceeds. The intensities of both carbonyl carbon species as well as those of both adsorbate oxygen species successively decrease and nearly drop to zero in the case of anhydride oxygen and carbonyl carbon at temperatures above 600 K. The total intensity of the olefinic carbon instead stays nearly constant between 200 and 600 K. The absence of carboxyl groups at 600 K indicates the absence of intact molecules in this temperature regime.

XPS of MA Deposited on ZnO(10$\bar{1}$0). Figure 4 shows the XPS results of the corresponding experiment performed on the ZnO-terminated ZnO(10$\bar{1}$0) surface. Here, the dosage amounted to 115 L at 160 K, yielding approximately one monolayer.

At 160 K, the XPS data in the C1s region are fitted using two lines of equal intensity located at the multilayer positions, i.e., at 286.3 and 290.0 eV. Good agreement with the experimental data is only achieved by introducing two additional lines at 288.5 and 285.1 eV, which are again of equal intensity. The appearance of two pairs of lines can be attributed to two different MA adsorbate species, which both exhibit the stoichiometry of intact molecules. The fit of the O1s spectrum contains two lines corresponding to anhydride (534.6 eV) and carbonyl oxygen (533.2 eV), respectively. The resulting adsorbate stoichiometry is consistent with the presence of intact molecules.

At 180 K, deviations from the original stoichiometry are seen. Similar to the fragmentation pathway observed in the case of Zn−ZnO, the original main C1s lines at 290.0 and 286.3 eV show a decrease, whereas the lines at 288.5 and 285.1 eV increase in relative intensity. The total intensity in the carbonyl carbon regime, however, decreases accompanied by a decrease of both O1s lines. The total intensity in the olefinic carbon regime remains unchanged. At 200 K, the changes become more pronounced, and in the O1s regime, preferential loss of the anhydride oxygen is evident. Again, the XPS results suggest a decomposition reaction involving the loss of carbonyl or carboxyl species. The XPS data also reveal that the decomposition is not complete after heating to 200 K. The adlayer contains decomposition fragments together with intact molecules.

In the temperature regime between 200 and 600 K, the decomposition continues, which leads to a further intensity decrease of the carbonyl carbon species and of the anhydride oxygen species. At 600 K, the line characteristic for anhydride oxygen vanishes which points toward total decomposition of MA. The resulting adsorbate layer consists of two different carbon species and oxygen.

XPS of MA Deposited on "Near-Stoichiometric" O−ZnO. The next section deals with the results obtained on the "near-stoichiometric" ZnO(000$\bar{1}$) sample. First, the experiment carried out on the crystal after standard preparation will be reported. In the following, the same experiment performed on the same crystal after pretreatment with atomic hydrogen will be discussed.

Figure 5 displays XP spectra of MA on the near-stoichiometric surface. Here, the dosage of 15 L at 140 K resulted in a coverage of approximately 3 layers. The multilayer is found to be stable up to 180 K. The multilayer desorption results in a monolayer coverage with the stoichiometry of intact MA at 200 K. As in the case of the surfaces discussed previously, the fit in the C1s region contains two pairs of lines, whereas the O1s regime is fitted using one line for the anhydride and the carbonyl species, respectively. The stoichiometry remains unchanged up to approximately 250 K. At this temperature, a slight intensity decrease can be observed for both carbonyl C1s lines as well as for the anhydride oxygen line. Heating to higher temperatures leads to a further intensity loss of these lines. Thus, the reaction

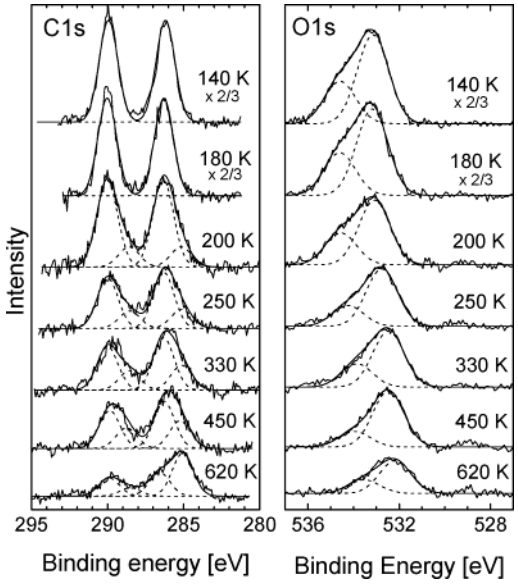

Figure 5. XPS series of a MA multilayer on the near-stoichiometric O−ZnO(000$\bar{1}$) crystal after standard preparation.

TABLE 2: Percentage of Undecomposed MA Derived from the C1s XPS Intensities at the Given Temperatures

surface termination	after spontaneous fragmentation	350 K	600 K
Zn−(0001)	200 K: 44%	23%	14%
(10$\bar{1}$0)	200 K: 49%	18%	11%
O−(000$\bar{1}$) (near-stoich.)	250 K: 71%	62%	39%
O−(000$\bar{1}$) (near-stoich., + atomic H)	220 K: 55%	27%	23%
O−(000$\bar{1}$) (defect-rich)	220 K: 56%	20%	no data

pathway observed on the near-stoichiometric O-terminated surface corresponds to that reported above for the Zn-terminated and the ZnO(10$\bar{1}$0) surfaces. However, compared to the latter surfaces the changes on the near-stoichiometric O−ZnO face are significantly less pronounced. At 620 K, there are still contributions of carbonyl carbon and anhydride oxygen, pointing toward a considerable amount of intact molecules on the surface (see Table 2).

Figure 6 shows the results of the same experiment, carried out on the near-stoichiometric O-terminated crystal after pretreatment with atomic hydrogen (1×10^{-6} mbar H_2 for 5 min). During this procedure the sample temperature was stabilized to 300 K. Atomic hydrogen is known to introduce defects in the surface and subsurface regimes by Zn−O bond cleavage.[31] Thus, an increase of the defect density was expected for this crystal.

After hydrogen adsorption, the crystal was cooled to 140 K and exposed to 15 L MA, leading to a coverage of 3.5 layers. As before, multilayer desorption is observed between 180 and 200 K, leaving an intact monolayer of MA on the surface. Again, four C1s lines can be distinguished in the monolayer regime. At 220 K, the typical changes characteristic for MA decomposition are observed in the C1s and O1s regions. Upon further heating, the degree of decomposition increases, which at 650 K yields non-carboxylic carbon as the main component on the surface. In addition, small amounts of anhydride oxygen as well as carbonyl carbon can still be detected, indicating that intact MA molecules are still present on the surface (see Table 2). Compared to the reactivity on the same crystal without

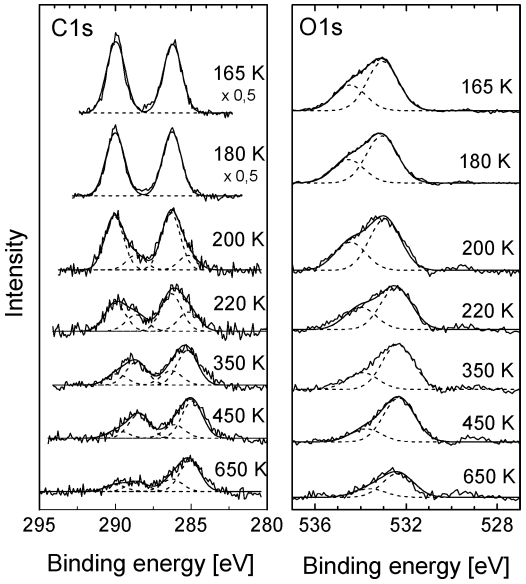

Figure 6. XPS series of MA on near-stoichiometric O−ZnO(000$\bar{1}$) after pretreatment of the crystal with atomic hydrogen. The exit angle of the photoelectrons was 20° with respect to the sample surface in this case.

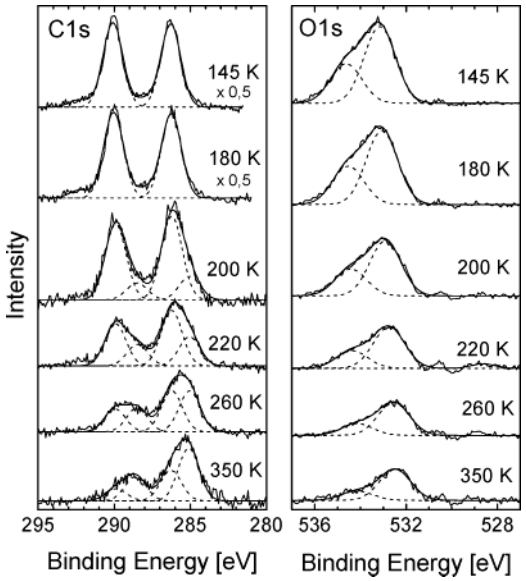

Figure 7. XPS series of a multilayer of MA deposited on the defect-rich O−ZnO(000$\bar{1}$) surface after standard preparation.

hydrogen pretreatment, the degree of decomposition achieved after hydrogen exposure is noticeably higher.

XPS of MA Deposited on "Defect-Rich" O−ZnO. The second O-terminated crystal under investigation was considered to exhibit a higher defect density than the crystal described above due to the fact that it had been under investigation for a significantly longer time and that exposures to atomic hydrogen had been applied several times.

Figure 7 shows the experimental results obtained for MA on this crystal in the temperature regime between 145 and 350 K. The dosage amounted to 100 L at 140 K, resulting in a coverage of 5 layers. Multilayer desorption occurs between 180 and 200 K, resulting in a mono- or bilayer with only slight deviations from the stoichiometry of intact MA. Increasing the temperature up to 220 K leads to an overall intensity decrease which yields a monolayer exhibiting the typical indications for MA decomposition. These involve loss of carbonyl or carboxyl groups. Upon further temperature increase, the fragmentation proceeds

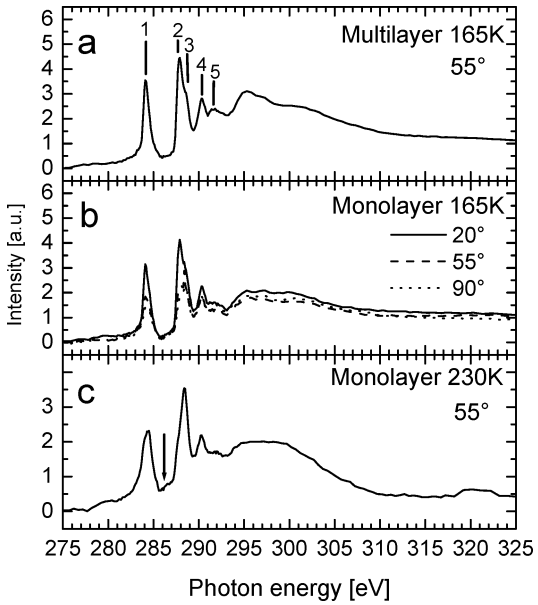

Figure 8. C1s NEXAFS spectra of the MA multilayer (a) and the monolayer at 165 K (b) as well as the partially decomposed monolayer at 230 K (c), recorded on the near-stoichiometric O face.The assignment of the π^* resonances 1−5 in spectrum a is given in Table I. The new resonance that appears in the spectrum of the decomposed monolayer (c) is marked by an arrow.

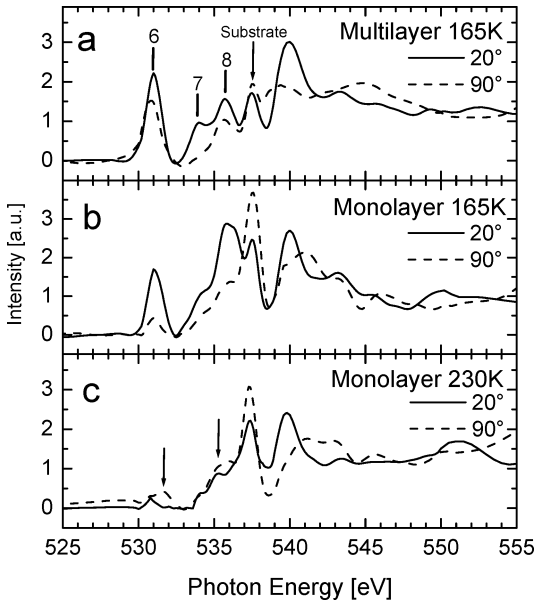

Figure 9. O1s NEXAFS spectra of the MA multilayer (a) and the monolayer at 165 K (b) as well as the partially decomposed monolayer at 230 K (c), recorded on the near-stoichiometric O face. The assignment of the π^* resonances 6−8 in spectrum a is given in Table 1. The new features that appear after decomposition are indicated by arrows in spectrum (c).

and, at 350 K, yields a decomposition degree which exceeds by far that obtained on the near stoichiometric O-terminated surface at 350 K (compare Table 2).

NEXAFS. *NEXAFS of MA on "Near-Stoichiometric" O−ZnO.* C1s and O1s NEXAFS measurements were performed on the near-stoichiometric O-terminated ZnO(000$\bar{1}$) crystal. In Figure 8, C1s NEXAFS spectra of an MA multilayer (a) and an MA monolayer (b) on this sample at 165 K are compared. In agreement with XPS data in both cases, intact molecules are present on the surface. The assignment of the resonances, given in Table 2, is in accordance with that of Lopez et al.[16]

Regarding the multilayer and monolayer spectra, no significant differences can be observed with respect to the position of the related resonances. Following Lopez et al.,[16] the π^* resonance at 284.0 eV ("π_1^*(C═C)") is assigned to transitions from the olefinic C1s level to the lowest unoccupied molecular orbital (LUMO). The adjacent resonance at 287.4 eV contains contributions from transitions of the olefinic C1s level into the LUMO+1 ("π_2^* (C═C)") as well as transitions of the carbonyl carbon level into the LUMO ("π_1^*(C═O)"). The shoulder of this line at 288.3 eV is caused by a π^* resonance resulting from transitions from the olefinic C1s level into the LUMO+2 ("π_3^*(C═C)"). The next line is attributed to a transition from the carbonyl carbon level again ("π_2^*(**C**═O)").

While in the case of the multilayer spectra no angular dependence could be observed, the π^* resonances of the monolayer spectra at 165 K show an angular dependence. The highest intensity is observed for grazing incidence and the lowest intensity in the case of normal incidence. The intensity ratio of the π^* resonances at 284.0 eV measured at normal and grazing incidence, respectively, yields an average tilt angle of 50° for the molecular plane with respect to the surface.

The analysis of the O1s NEXAFS spectra measured on the near-stoichiometric crystal (see Figure 9a−c) was complicated by several factors. First, the adsorbate signal intensities were weak compared to those of the oxygen containing substrate. Furthermore, the substrate signals did not completely disappear in the difference spectra obtained by subtraction of the clean substrate spectra. This gave rise to the intense (angular dependent) resonance at 537.5 eV. Technical problems during data acquisition also complicated the normalization of the spectra.

However, in accordance with the NEXAFS data of Lopez et al.,[16] three π^* resonances can be identified for the multilayer as well as for the monolayer spectra at 165 K (see Figure 9a,b) at 531.0, 534.7, and 535.6 eV resulting from transitions from the carbonyl O1s level to the LUMO ("π_1^*(C═O)"), to the LUMO+1 (("π_2^*(C═O)"), and the LUMO+2 ("π_3^*(C═O)"). No angular dependence could be observed in the case of the multilayer spectra. For the monolayer the spectra reveal a dichroism of the NEXAFS resonance intensities which indicates a tilt angle of 35° for the molecular plane with respect to the surface. This value slightly deviates from the tilt angle determined from the C1s NEXAFS spectra, which amounts to 50°. This variation of the tilt angles is most likely due to the difficulties of the normalization of the O1s NEXAFS spectra. The good agreement of multilayer and monolayer spectra, where no additional features can be observed in the π^* regime, rules out a significant distortion of the molecules. The substrate related resonance at 537.5 eV becomes more pronounced in the latter case.

The monolayer (displayed in Figures 8b and 9b, respectively) was then heated to 230 K to induce the fragmentation of MA. The resulting C1s and O1s NEXAFS spectra are displayed in Figures 8c and 9c, respectively.

Comparison of the C1s-NEXAFS spectrum in Figure 8c with that of the intact monolayer in Figure 8b reveals changes in the relative intensities of the resonances. A decrease of the π_1^*(C═C) resonance at 284.0 eV as well as a decrease of the resonance at 287.4 eV (π_2^*(C═C) + π_1^*(C═O)) and the π_2^*(C═O) resonance is observed, whereas the relative intensity of the π_3^*(C═C) resonance at 288.3 eV is increased. A weak new feature appears at 286.5 eV. As is evident from the XPS results, at 230 K, only a fraction of the monolayer is decomposed so that the NEXAFS data correspond to a superposition of

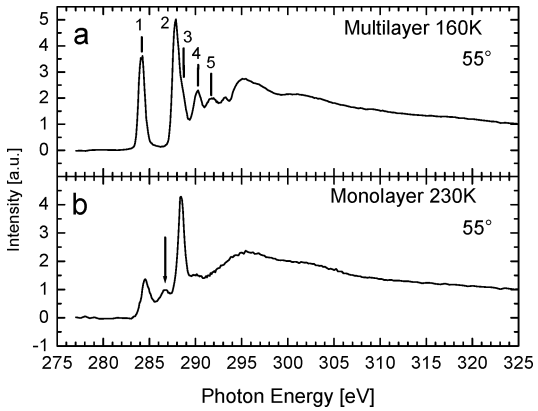

Figure 10. C1s NEXAFS spectra of the MA multilayer at 160 K (a) and the partially decomposed monolayer at 230 K (b) on the defect-rich O−ZnO surface. The assignment of the π^* resonances 1−5 in spectrum a is given in Table 1. The new resonance that appears in the spectrum of the decomposed monolayer (b) is marked by an arrow.

spectra for both intact MA and the decomposed (decarboxylated) species. The similarities between the NEXAFS spectra of the intact monolayer at 165 K and the monolayer at 230 K are due to the large fraction of intact MA molecules.

Regarding the temperature induced changes in the O1s NEXAFS spectrum measured on the near-stoichiometric sample, the most noticeable change is the drastic intensity decrease of the original π^* resonances characteristic for intact MA. Two weak new π^* resonances arise at 531.5 and 535.3 eV, which can be attributed to the fragmentation products formed. The low intensities of the carbonyl-related O1s NEXAFS resonances is in accordance with the loss of carboxyl or carbonyl groups.

NEXAFS of MA on "defect-rich" O−ZnO. As is evident from the XPS data, for the defect-rich surface the degree of decomposition at 230 K is significantly higher than for the near-stoichiometric surface. In Figure 10, C1s NEXAFS spectra of the multilayer at 160 K (a) and the monolayer (b), prepared by heating the multilayer to 230 K, are displayed. The changes that occur upon this temperature rise are similar to those observed for the near-stoichiometric surface. In this case, however, the changes are clearly more pronounced which can be correlated to the larger fraction of molecules decomposed.

Surface Composition. Regarding the formation of surface species by decomposition of MA the question arises as to whether the surface composition remains unchanged or whether surface oxygen (which is mobile, especially at elevated temperatures[32,33]) participates in the surface reaction. Therefore, the stoichiometry of the substrate, given by the ratio N_O/N_{Zn}, was determined from the intensities of the substrate XPS lines at 530.7 eV (O1s) and 1021.8 eV ($Zn2p_{3/2}$). N_O and N_{Zn} are the numbers of O and Zn atoms in the ZnO sample, respectively. A constant N_O/N_{Zn} ratio, amounting to 1.0, is expected if the surface is not affected by the surface reaction. When analyzing the experimental data, however, it has to be considered that in the presence of an organic adlayer on the surface the O1s and C1s photoelectrons are attenuated differently. If the surface is covered by an adsorbate layer of thickness d, the measured intensities of the substrate XPS-signals, I_{Zn} and I_O, are related to the intensities of the clean substrate, $I_{Zn,clean}$ and $I_{O,clean}$, by

$$I_{Zn} = I_{Zn,clean} \exp[-d/\lambda_{Zn}] \text{ and } I_O = I_{O,clean} \exp[-d/\lambda_0]$$

λ_{Zn} and λ_0 are the inelastic mean free paths of the corresponding photoelectrons.

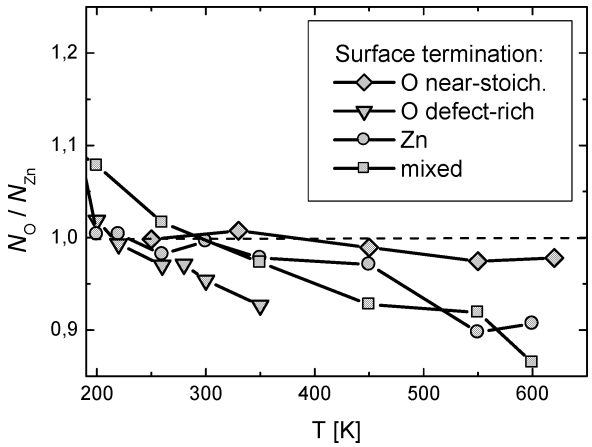

Figure 11. Plot of N_O/N_{Zn} versus temperature. A constant ratio of 1 (dotted line) is expected in the case that the surface composition is not changed by the decomposition reaction.

By connecting both equations one yields

$$I_{0,clean}/I_{Zn,clean} = I_0/I_{Zn} \exp[d(1/\lambda_o - 1/\lambda_{Zn})]$$

$I_{0,clean}/I_{Zn,clean}$ is the XPS intensity ratio that would be expected in the absence of the adsorbate. The layer thickness d was estimated by setting the coverage of the ZnO(10−10) surface at 200 K to a monolayer and assuming that the layer thickness is proportional to the intensity of the adsorbate C1s signal. From the $I_{0,clean}/I_{Zn,clean}$ ratio the stoichiometry of the adsorbate, N_O/N_{Zn}, can be calculated using

$$N_0/N_{Zn} = f\ I_{0,clean}/I_{Zn,clean}$$

where f is a constant factor that can be evaluated from the known $I_{0,clean}/I_{Zn,clean}$ ratio of the clean sample with a normalization of N_0/N_{Zn} to 1.

If the surface stoichiometry is not changed during the decomposition reaction, the calculated ratio is expected to be unity. Figure 11 shows the results of this analysis for the near-stoichiometric and defect-rich O-faces as well as for the Zn face and the (10−10) face in the temperature range between 200 and 650 K.

A nearly constant O/Zn-ratio was observed for the near-stoichioimetric O-terminated sample. The ratio is found to be close to one in the lower temperature regime and decreases only slightly above 400 K. Regarding the defect-rich O-terminated sample, the ratio is in the range of 1 below 200 K, and drops to 0.93 between 220 and 350 K, hence showing a significantly different behavior than the near-stoichiometric sample. The stoichiometry of the Zn-terminated surface is found to be close to unity below 220 K and slightly below unity up to 450 K. Above 450 K, a strong decrease to approximately 0.9 is observed. In the case of the (10−10)-terminated surface, the stoichiometric ratio clearly deviates from unity above 300 K and decreases to a value of 0.86 at 600 K.

Discussion

It is evident from the data presented above that the temperature-induced fragmentation of MA follows the same pathway on all three ZnO surfaces, although the degree of fragmentation varies. The characteristic changes observed in the XPS data due to the fragmentation involve a decrease of the carbonyl-related C1s-lines as well as a decrease of the anhydride oxygen line. From the decrease of the carbonyl carbon species a partial decarboxylation or decarbonylation reaction can be concluded.

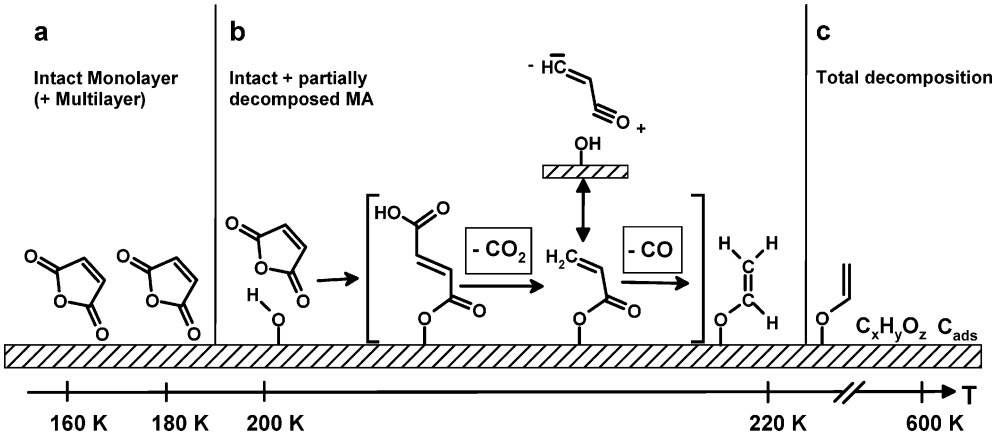

Figure 12. General model for the temperature induced fragmentation of MA on ZnO surfaces. Part (a) shows the low-temperature regime, where the multilayer is stable and intact MA molecules are present on the surface. Part (b) demonstrates how a fraction of the MA monolayer undergoes decomposition. The first step is assumed to be a ring opening promoted by surface hydroxyl groups. The reaction then proceeds via intermediary formed decarboxylation and decarbonylation products, respectively, giving rise to stable surface species. In correlation with the spectroscopic data ethenolate can be regarded as a possible reaction product. Also more complex surface reactions such as oligomeriztation and polymerization processes have to be considered. Part (c) depicts the high-temperature regime where total decomposition becomes favored.

In both cases the decomposition is accompanied by a ring opening which leads to the disappearance of the anhydride oxygen species. The detection of anhydride oxygen can thus be attributed to the presence of intact MA molecules. The partial loss of CO or CO_2 is also in agreement with the NEXAFS data where the disappearance of the π^* resonances related to the carboxyl group was observed for the decomposed monolayer. This does not exclude the existence of non-carboxylic, σ-bonded C−O groups.

Large variations were found regarding the degree of decomposition achieved on the different ZnO surfaces. In the case of the O-terminated surfaces, the highest reactivity was found on the defect-rich surface, and the lowest was found on the near-stoichiometric surface without hydrogen pretreatment. The reactivity of the near-stoichiometric surface was found to be slightly increased after pretreatment of the sample with atomic hydrogen, thus emphasizing the role of defects for the reactivity toward MA. The degrees of MA decomposition on the Zn−ZnO and ZnO($10\bar{1}0$) surfaces are comparable. They exceed those observed for the near-stoichiometric crystal but are still lower than that of the defect-rich O face.

The decomposition reaction of MA on ZnO can generally be attributed to two different temperature regimes. On the basis of the XPS and NEXAFS data and considering the temperatures where the different species are observed, we propose a model for the decomposition pathway and the chemical nature of the decomposition products which is displayed in Figure 12.

Intact Molecules: <180−220 K. Scheme a in Figure 12 represents the temperature regime below 200/220 K, where the stoichiometry corresponds to that of intact MA molecules. The O1s XP spectra show two lines, corresponding to carboxyl and anhydride oxygen, respectively, with a ratio of 2:1. In the C1s regions, two main lines of equal intensity are detected, which are related to olefinic (285.7 eV) and carbonyl carbon (289.4 eV), respectively. The presence of the two additional smaller C1s lines, which are of equal intensity, too, can be attributed to a fraction of MA molecules in the first adsorbate layer which are bound to the surface in a different adsorption mode than the majority of molecules, e.g., through ring opening. However, the presence of the π_1^*(C═C) resonance in the C1s NEXAFS spectrum of the monolayer reveals that the double bond of the MA molecule is conserved and that a di-σ-bond to the surface (as observed on Si(100)[16,17]) can be ruled out. From the angular dependence of the NEXAFS resonances, an orientation of the molecular plane parallel to the surface can be ruled out. Instead, an average tilt angle of 42° was observed for the molecular plane with respect to the surface plane. For clarity reasons, in Figure 12 the intact MA molecules are depicted with their molecular plane parallel to the surafce normal.

Spontaneous Fragmentation: 180−220 K. In the temperature range between 180 and 220 K, a surface-induced fragmentation is observed (see Figure 12b), leading to a drastic intensity change of the relative C1s and O1s peak intensities. An exception is the near-stoichiometric O-terminated surface where no spontaneous fragmentation of the MA was observed in this temperature regime.

From the intensity changes observed in the XP spectra, a partial decarboxylation or decarbonylation can be derived. In the C1s region, the carbonyl related main line decreases in intensity, and in the O1s region, both lines decrease (decarbonylation leads to transformation of the anhydride O species into a carboxyl-like O species, decarboxylation also removes the anhydride O atom).

A detailed analysis of the C1s XP spectra recorded on the different surfaces after the spontaneous fragmentation indicates the coexistence of intact and decomposed molecules.

The C1s peak at 290.0 eV can be exclusively attributed to the carbonyl carbon species of intact MA. A peak of the same intensity is expected for the olefinic carbon species of intact MA at 286.3 eV. Therefore, the percentage of intact MA molecules in the total spectral C1s intensity was estimated by comparing twice the intensity of the peak at 290.0 eV to the total measured C1s intensity. The results are summarized in Table 2.

Inspection of Table 2 reveals that the degree of decomposition is highest on the Zn-terminated and ZnO(10−10) surfaces and lowest on the near-stoichiometric O-terminated surface after standard preparation. On the basis of these observations, we speculate that the spontaneous decomposition reaction only takes place in the vicinity of active sites on the surface, e.g., defects such as oxygen vacancies.

The temperature of the spontaneous fragmentation was found to depend on the surface termination and on the defect density of the crystals. In the case of the hydrogen-pretreated near-stoichiometric and the defect-rich O-terminated samples, the spontaneous fragmentation was observed between 200 and 220

K. In the case of the Zn- and ZnO-terminated crystals, fragmentation was already observed below 200 K, where it is accompanied by multilayer desorption.

The coexistence of molecules and fragments is corroborated by the NEXAFS data, which show a decrease of all carboxyl-related C1s NEXAFS resonances when the MA adlayer is heated to temperatures of about 200 K. Furthermore, the π_1^*(C═C) resonance decreases in intensity and a new feature arises at 286.5 eV. Since XPS reveals a nearly constant intensity of the olefinic carbon species, a desorption of such species can be ruled out. Instead, either a rehybridization of the C═C double bond or a shift of the original π_1^*(C═C) resonance has to be considered. This might also be the reason for the new feature at 286.5 eV observed in the NEXAFS spectrum.

Regarding the O1s NEXAFS data, the intensities of the of the π_1^*(C═O), π_2^*(C═O), and π_3^*(C═O) resonances are strongly reduced, which can partly be explained by the loss of carboxyl/carbonyl groups, which was derived from the XPS data. Two weak new features emerge which can be attributed to carboxyl or carbonyl groups in the formed MA fragments. However, the decrease of the O1s π^* resonance intensities observed upon decomposition is too pronounced to be solely explained by the partial loss of C═O groups. In fact, the analysis of the XPS data reveals that the adsorbed layer on the near-stoichiometric O-terminated crystal still contains about 70% of CO groups in the corresponding temperature regime. Hence, σ-bonded C−O groups have to be assumed for the majority of the adsorbed species instead of the original π-bonded C═O groups. The change of the bonding state of the CO group provides evidence that the oxygen-containing part of the MA molecule preferentially interacts with the surface.

Also, more complex surface reactions leading to a rearrangement of the adsorbed species or to polymerization can be considered. Saturation of cleaved bonds can either occur by bonding to surface oxygen, by oligomerization or by uptake of hydrogen. It is likely that hydrogen atoms are available on the surfaces due to the characteristic property of ZnO to form hydroxyl groups even under UHV conditions.[26−28] Also the adsorbed MA species can act as a source of hydrogen if surface-promoted C−H bond breaking takes place.[23] Scheme b in Figure 12 proposes several intermediate species resulting from the decomposition process around 200 K which are consistent with the experimental data.

Toward Total Decomposition: 200−600 K. Between 200 and 600 K (and above), the degree of MA decomposition increases with temperature on all surfaces. On the near-stoichiomertic crystal, where no spontaneous fragmentation was observed, the decomposition reaction slowly starts at around 250 K. At temperatures above 600 K, the fraction of intact MA molecules nearly drops to zero on the Zn−ZnO and ZnO($10\bar{1}0$) surfaces. The intensity contributions of intact MA molecules to the total C1s intensities at 350 and 600 K, respectively, are compared in Table 2.

The species present on the ZnO surfaces at 600 K give rise to two main C1s lines with binding energies of 284.5 and 286.0 eV, respectively, and a main oxygen line at 532.5 eV. The C1s species with the higher binding energy and the oxygen species would be consistent with the presence of a single bonded C−O unit. In the case of the near-stoichiometric O-terminated ZnO surfaces, the spectra reveal also significant contributions of carbon species with a binding energy of 290.0 eV and an oxygen species with a binding energy of about 534 eV. These signals would be consistent with the presence of small amounts of nondissociated molecules (see Table 2). Scheme c in Figure 12 shows several species which are consistent with the photoelectron spectroscopy data recorded in this temperature regime.

Stoichiometric Changes of the ZnO Surfaces during MA Decomposition. With regard to catalytic processes occurring at the surfaces of ZnO substrates, it is of key importance to investigate the contribution of substrate oxygen to chemical reactions occurring at the surface.

To investigate whether substrate oxygen is consumed in the progress of the MA decomposition, we have plotted the substrate O to substrate Zn ratio as a function of surface temperature, see Figure 11. A nearly constant O/Zn ratio close to unity was observed for the near-stoichioimetric O-terminated sample, indicating that the stoichiometry of the surface remains essentially unchanged by the surface reaction. A slight decrease of the oxygen content at high temperatures, which was also observed for the near-stoichiometric sample, can be related to an oxygen loss in the surface region of the crystal, which is connected to the increased mobility of O atoms at high temperature.[32,33] Note that in previous work[26,28] it has been observed that heating the hydroxylated O−ZnO surfaces to temperatures above 650 K results in a formation of a clean (3×1) reconstructed surface which is accompanied by an oxygen loss. The current model for the reconstructed (3×1) surface proposes an ordered array of oxygen vacancies.[26]

Regarding the defect-rich O-terminated surface, a strong decrease of the O/Zn ratio is evident for temperatures between 280 and 350 K. Since this temperature range is too low to cause substrate oxygen loss,[34] e.g., by desorption of water,[26] the explanations given above do not apply for the defect-rich surface. However, the decrease of the O/Zn ratio is significantly larger on the defect-rich surface than on the near-stoichiometric surface. The apparent oxygen loss of the defect-rich surface can be explained by the idea that the missing oxygen atoms are still present on the surface but do not contribute to the substrate O1s line. This is the case, when the interaction of the surface oxygen atoms with the surface species is so strong that it leads to a chemical shift which clearly deviates from that of the substrate O species. Hence, these results strongly suggest that the chemical state of the defect-rich O-terminated face is significantly changed due to consumption of substrate oxygen by the surface reaction.

A similar behavior is observed for the Zn-terminated Zn−ZnO surface and for the ZnO($10\bar{1}0$) surface. Around 600 K, both samples exhibit O/Zn ratios in the range of 0.9. Again, the apparent loss of surface oxygen can be attributed to surface oxygen atoms that take part in the formation of surface species which causes a shift in the XPS binding energy. This interpretation is in accord with the observation that oxygen is detected by XPS as a component of the adsorbed surface species in the high-temperature regime.

With regard to the Zn atoms, it has to be noted that the XPS binding energy of the Zn2p lines is not a sensitive measure of the chemical state of the Zn atoms.[35] Consequently, the present XPS data do not rule out the possibility that Zn atoms are removed from the surface and included in some of the molecular fragments on the surface as well. We consider, however, this possibility as highly unlikely.

On the basis of the observations described above, we can draw the conclusion that significant decomposition of the MA molecules on all surfaces correlates with pronounced changes of the surface stoichiometry, i.e., significant loss of substrate oxygen atoms. Among the different types of ZnO substrates studied in the present work, the near-stoichiometric surface showed the lowest reactivity toward MA, whereas a considerable

degree of decomposition was observed on the defect-rich O-terminated surface as well as on the Zn-terminated surface and on the $(10\bar{1}0)$ surface.

Conclusions

The polar ZnO(0001) and ZnO$(000\bar{1})$ surfaces as well as the nonpolar ZnO(10−10) surface are active for MA decomposition. On all surfaces, the first decomposition step, involving decarboxylation or decarbonylation, was observed around 200 K. The decomposition degree was found to increase with temperature, proceeding toward total decomposition around 600 K. Above 600 K, carbonaceous oxygen containing species are still present on the surface.

In the case of the O-terminated surfaces, a correlation between defect density and reactivity could be established. Although the near-stoichiometric surfaces exhibited only low reactivity, the defect-rich surface showed the highest reactivity of all samples.

Apparently, the fragmentation of the MA molecule is induced by the interaction of the anhydride group with the surface, since the content of C═O double bonds in the monolayer is strongly decreased after the first decomposition step. This is not solely due to the partial loss of CO/CO_2 groups, but also a result of rehybridization of the remaining C═O groups into σ-bonded C−O species. The reaction pathway involves ring opening, which might be regarded as the first reaction step induced by the interaction of the anhydride group of the MA molecule with the surface. Acid−base pairs can generally be considered to be the active surface sites, since they are capable of promoting the cleavage of the anhydride bond. However, the exact nature of the centers active for MA decomposition is not known at present. In the case of the O-terminated ZnO face, it was shown that the introduction of defects by treatment with atomic hydrogen enhances the reactivity. Since H radicals are capable of cleaving ZnO bonds, the increased reactivity can possibly be related to substrate atoms with a decreased coordination number.

For the ZnO surfaces exhibiting the highest reactivity toward MA, namely the defect-rich O-face, the Zn face and the $(10\bar{1}0)$ face, it was shown that the chemical state of the surfaces is changed upon the decomposition reaction. Obviously, substrate oxygen atoms are involved in the surface reaction, possibly stabilizing the formed surface species. The nature of the active sites is not known, but the ability of the surface to donate oxygen atoms seems to be a determining factor for the reactivity toward MA.

Regarding the role of ZnO in Cu/ZnO catalysts, changes of the chemical state of the ZnO surfaces can also affect the chemical properties of the copper particles which are in contact with the ZnO phase. Also the wetting properties and hence the morphology of a catalyst might be changed due to the modification of the ZnO surface.[36] Since the total decomposition of MA on ZnO leads to carbonaceous surface species that are stable even above 600 K, catalyst coking has to be taken into account. Furthermore, the ability of ZnO to decompose MA can contribute to the formation of byproducts.

References and Notes

(1) Weissermehl, K.; Arpe, H.-J. *Industrial organic chemistry*; VCH Wiley: Weinheim, Germany, 1978.
(2) Brownstein, A. M. *Chemtec* **1991**, *8*, 506.
(3) Brownstein, A. M.; List, H. L. *Hydrocarbon Process.* **1977**, *9*, 159.
(4) Herrmann, U.; Emig, G. *Chem. Eng. Technol.* **1998**, *21*, 3.
(5) Schlander, J. H.; Turek, T. *Ind. Eng. Chem. Res.* **1999**, *38*, 1264.
(6) Messori, M.; Vaccari, A. *J. Catal.* **1994**, *150*, 177.
(7) Herrmann, U.; Emig, G. *Ind. Eng. Chem. Res.* **1997**, *36*, 2885.
(8) Herrmann, U.; Emig, G. *Ind. Eng. Chem. Res.* **1998**, *37*, 759.
(9) Castiglioni, G. L.; Fumagalli, C.; Guercio, A.; Lancia, R.; Messori, M.; Stefani, G.; Vaccari, A. *Wissenschaft Technik* **1994**, *47*, 146.
(10) Castiglioni, G. L.; Fumagalli, C.; Guercio, A.; Lancia, R.; Messori, M.; Vaccari, A. *Wissenschaft Technik* **1994**, *47*, 33.
(11) Ohlinger, C.; Kraushaar-Czarnetzki, B. *Chem. Eng. Sci.* **2003**, *58*, 1453.
(12) Kanetake, J.; Asano, T.; Masamune, S. *Ind. Eng. Chem.* **1970**, *62*, 24.
(13) Wilson, J. N.; Titheridge, J.; Idriss, H. *J. Vac. Sci. Technol. A* **2000**, *18*, 1887.
(14) Xu, C.; Goodman, D. W. *Langmuir* **1996**, *12*, 1807.
(15) Pallassana, V.; Neurock, M.; Coulston, G. *Catal. Today* **1999**, *50*, 589.
(16) Lopez, A.; Bitzer, T.; Heller, T.; Richardson, N. V. *Surf. Sci.* **2001**, *477*, 219.
(17) Bitzer, T.; Rada, T.; Richardson, N. V. *J. Phys. Chem. B* **2001**, *105*, 4535.
(18) Akhter, S.; Lui, K.; Kung, H. H. *J. Phys. Chem.* **1985**, *89*, 1958.
(19) Akhter, S.; Cheng, W. H.; Lui, K.; Kung, H. H. *J. Catal.* **1984**, *85*, 437.
(20) Crook, S.; Dhariwal, H.; Thornton, G. *Surf. Sci.* **1997**, *382*, 19.
(21) Petrie, W. T.; Vohs, J. M. *Surf. Sci.* **1991**, *245*, 315.
(22) Vohs, J. M.; Barteau, M. A. *Surf. Sci.* **1986**, *176*, 91.
(23) Vohs, J. M.; Barteau, M. A. *J. Phys. Chem.* **1987**, *91*, 4766.
(24) Vohs, J. M.; Barteau, M. A. *Surf. Sci.* **1988**, *201*, 481.
(25) Vohs, J. M.; Barteau, M. A. *J. Electron Spectrosc. Relat. Phenom.* **1989**, *49*, 87.
(26) Kunat, M.; Gil Girol, S.; Becker, T.; Burghaus, U.; Wöll, C. *Phys. Rev. B* **2002**, *66*, 081402.
(27) Staemmler, V.; Fink, K.; Meyer, B.; Marx, D.; Kunat, M.; Burghaus, U.; Gil Girol, S.; Wöll, Ch. *Phys. Rev. Lett.* **2003**, *90*, 106102.
(28) Kunat, M.; Gil Girol, S.; Burghaus, U.; Wöll, Ch. *J. Phys. Chem. B* **2003**.
(29) Seah, M. P.; Dench, W. A. *Practical surface analysis*; John Wiley & Sons: New York, 1990.
(30) Tanuma, S.; Powell, C. J.; Penn, D. R. *Surf. Interface Anal.* **1993**, *20*, 77.
(31) Becker, T.; Hövel, S.; Kunat, M.; Boas, C.; Burghaus, U.; Wöll, C. *Surf. Sci.* **2001**, *486*, L502.
(32) Göpel, W.; Lampe, U. *Phys. Rev. B* **1980**, *22*, 6447.
(33) Jacobi, K.; Zwicker, G.; Gutmann, A. *Surf. Sci.* **1984**, *141*, 109.
(34) Kohl, D.; Henzler, M.; Heiland, G. *Surf. Sci.* **1974**, *41*, 403.
(35) Rössler, N.; Staemmler, V. *Phys. Chem. Chem. Phys.* **2003**, *5*, 3580.
(36) Topsøe, N.-Y.; Topsøe, H. *J. Mol. Catal. A* **1999**, *141*, 95.